Afshar Vahid, Shahraam; Kalosha, V. P.; Bao, Xiaoyi; Chen, L.
Enhancement of stimulated Brillouin scattering of higher-order acoustic modes in single-mode optical fiber, *Optics Letters*, 2005; 30 (20):2685-2687.

Enhancement of stimulated Brillouin scattering of higher-order acoustic modes in single-mode optical fiber

Shahraam Afshar V.,* V. P. Kalosha, Xiaoyi Bao, and Liang Chen

Fiber Optics Group, Department of Physics, University of Ottawa, 150 Louis Pasteur, Ottawa, Ontario K1N 6N5, Canada

Received April 11, 2005; revised manuscript received June 2, 2005; accepted June 4, 2005

Solving the elastic wave equation exactly for a GeO_2-doped silica fiber with a steplike distribution of the longitudinal and shear velocities and density, we have obtained the dispersion, attenuation, and fields of the leaky acoustic modes supported by the fiber. We have developed a model for stimulated Brillouin scattering of these modes in a pump–probe configuration and provided their Brillouin gains and frequencies for an extended range of core sizes and GeO_2 doping. Parameter ranges close to cutoff of the acoustic modes and pump depletion enhance the ratio of higher-order peaks to the main peak in the Brillouin spectrum and are suitable for simultaneous strain–temperature sensing. © 2005 Optical Society of America

OCIS codes: 290.5830, 060.4370, 060.2370.

The stimulated Brillouin scattering (SBS) process has been both considered a limiting factor for optical communication and utilized advantageously (in optical amplification, Brillouin lasers, and distributed strain–temperature sensing)[1–3] in optical fibers. Owing to its wide range of applications, it is very important to design optical fibers with specific Brillouin gain spectra (BGS) having certain numbers of peaks corresponding to higher-order acoustic modes with certain frequencies, linewidths, and thresholds. A specific application is distributed, Brillouin-based fiber optic sensors, for which multipeak BGS can be potentially employed for simultaneous strain and temperature measurements.[4,5] For this, the ratio of higher-order peaks relative to the main peak should be enhanced for simultaneous measurements.

SBS in optical fibers is due to the interaction of the laser beam with different acoustic modes supported by the fibers. Because of the solid-state nature of the glass materials, these modes are defined by the spatial distribution of the longitudinal, V_L, and shear, V_S, velocities and density, ρ, of the core and cladding materials. The studies of higher-order acoustic modes and their features in the BGS are limited either to the assumptions $V_{S1}=V_{S2}$ and $\rho_1=\rho_2$ (indices 1 and 2 refer to core and cladding, respectively) or to specific parameter sets of particular fibers under the undepleted regime.[6–8] Considering the current advanced fiber fabrication technology, especially for microstructured fibers, a study of SBS of higher-order acoustic modes for a distribution of V_L, V_S, and ρ involving pump depletion (e.g., pump–probe SBS amplification) and subnanosecond pulses is required.

Here we present a model of SBS in a pump–probe scheme, which includes exact solutions for acoustic modes in optical fibers with steplike variations of V_L, V_S, and ρ in the core and infinitely thick cladding as well as the pump depletion and transient regime. We study the dispersion, relative gains, and the frequency shifts of these modes as a function of fiber and laser beam parameters. It is shown that the acoustic modes are leaky, where the attenuation due to leakage is a periodic function of acoustic frequency. Depending on fiber parameters and acoustic frequency, the leakage attenuation can result in a phonon lifetime of ~20 ns, which is comparable with the material phonon lifetime. We have found that fibers close to the cutoff of higher-order acoustic modes and under the saturation regime of pump–probe Brillouin scattering, where the pump is depleted by interaction with the fundamental acoustic mode, exhibit the maximum ratio of higher-order peaks relative to the main peak.

The model is based on two wave equations for the optical Stokes and pump fields, respectively, $E_s=(1/2)A_s(\mathbf{r},t)\exp i(\omega_s t-\beta_s z)+\text{c.c.}$ and $E_p=(1/2)A_p(\mathbf{r},t)\exp i(\omega_p t+\beta_p z)+\text{c.c.}$, coupled to an elastic wave equation for the acoustic field $E_q=(1/2)A_q(\mathbf{r},t)\exp i(\omega_q t+\beta_q z)+\text{c.c.}$ With the slowly varying envelope approximation and from energy–momentum conservation laws for the frequencies and propagation constants, $\omega_p=\omega_s+\omega_q$ and $\beta_p=\beta_q-\beta_s$, the equations for the optical fields can be written as

$$(\hat{T}_j+\hat{P}_j)A_j=\hat{N}_j \qquad (j=s,p). \tag{1}$$

Here $\hat{T}_{s,p}=\nabla_t^2+(n^2k_{s,p}^2-\beta_{s,p}^2)$ are the transverse operators, $\hat{P}_{s,p}=2i\beta_{s,p}\partial_z-2i\omega_{s,p}(n/c)^2\partial_t$ are the longitudinal propagation operators, and $\hat{N}_s=-(\gamma/2\rho_0c^2)\omega_s^2A_pA_q^*$, $\hat{N}_p=-(\gamma/2\rho_0c^2)\omega_p^2A_sA_q$ are the nonlinear operators that describe the interaction between the acoustic and the optical fields, where ∇_t^2 is the transverse Laplacian, $n(x,y)$ is the refractive index profile, γ is the electrostrictive coefficient, ρ_0 is the average density, and c and $k_{s,p}$ are the speed of light and wavenumbers, respectively. We consider silica fibers with GeO_2-doped cores, where n_1, V_{L1}, V_{S1}, and ρ_1 change linearly with doping[9] Δ ($V_{L1}<V_{L2}$ and $V_{S1}<V_{S2}$). We use Waldron's expressions[10] for the vectorial elastic wave equation for the axially symmetric displacement field $\mathbf{u}$, consider the boundary conditions for $\mathbf{u}$ and stress tensor

0146-9592/05/202685-3/$15.00

fields **T** at the core–cladding interface, and solve the resulting complex characteristic equation for the propagation constants of the acoustic modes. It is found that the acoustic modes are leaky, radiating energy in the transverse direction into the cladding, and show oscillations in displacement fields inside the core (Fig. 1). We have labeled these modes LR_η to indicate the coupling of the longitudinal and radial displacements. Comparing the dispersion curves for the case $V_{S1} \neq V_{S2}$ and $\rho_1 \neq \rho_2$ with usually assumed case $V_{S1}=V_{S2}$ and $\rho_1=\rho_2$ (Ref. 6) shows differences of the order of 5–50 MHz in the corresponding Brillouin frequencies, depending on the core radius, doping, and mode number [Fig. 1(a)]. This may explain the discrepancy between experimental and numerical values of the Brillouin frequencies.[6,3]

By examining the displacement fields, we note that the acoustic wave can be well approximated as a scalar field, in terms of change in the density, by $E_q/\rho_0 = \nabla \cdot \mathbf{u} \approx i\beta_q u_z$. By the decomposition method (Ref. 11 and references therein) the acoustic field A_q is expanded as $A_q=\Sigma_\eta a_\eta(z,t)F_\eta(r)$, where F_η are the longitudinal components of LR_η. Considering single-mode fibers with optical fields $A_j=a_j(z,t)F(r)$, where F is the transverse optical mode satisfying $\hat{T}_j F=0$, a dynamic equation for the amplitudes a_η is

$$(\partial_t + \Gamma_\eta)a_\eta = -(i\gamma\beta_\eta^2/64\pi\omega_q)a_p a_s^* \int_0^\infty F^2 F_\eta^* r\,dr, \quad (2)$$

where $\Gamma_\eta=\Gamma_\eta'/2-i(\Omega_{B\eta}-\omega_q)$ is the detuning term in which $\Omega_{B\eta}$ is the Brillouin frequency, $\Gamma_\eta'=1/\tau_\eta$ (τ_η is the phonon lifetime corresponding to the ηth mode) represents the attenuation of the acoustic mode η due to absorption. However, for $V_{S1} \neq V_{S2}$ there is another attenuation mechanism that is due to the leaky nature of the acoustic modes. This attenuation is a periodic function of the acoustic frequency [Fig. 1(b)], and its magnitude and period increase as the core radius decreases. Also, decreasing doping increases the period and reduces the magnitude of the attenuation. For comparison, the attenuation due to absorption is of the order of $2-3\times10^4\ m^{-1}$ for the acoustic frequency 10 GHz. As a result, BGS at different Brillouin frequencies broadens, since the effective phonon lifetime for each mode is $1/\tau_{eff}=1/\tau_\eta+1/\tau_{leak}$, where τ_{leak} is the phonon lifetime due to leakage of the modes into the transverse directions.

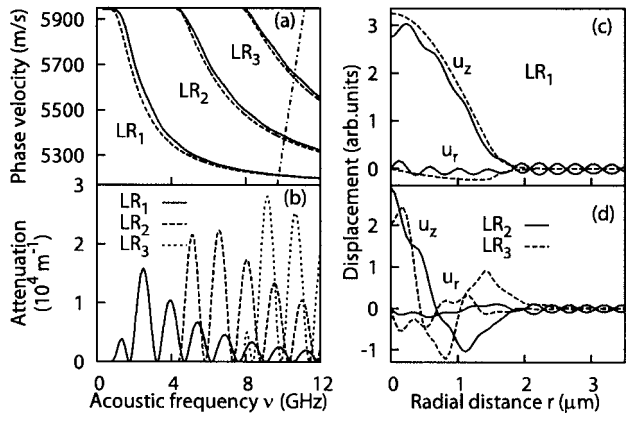

Fig. 1. (a) Dispersion, (b) attenuation due to leakage, (c) and (d) displacement fields for acoustic modes in a fiber with the core radius $R=1.5\ \mu m$ and doping $\Delta=18$ wt. % at wavelength 1.55 μm. The dashed curves in (a) and (c) are drawn for the case $V_{S1}=V_{S2}$ and $\rho_1=\rho_2$. The dotted–dashed line in (a) is $V=\pi\nu/\beta_p$, and its intersections give the Brillouin frequencies Ω_{B1-B3}.

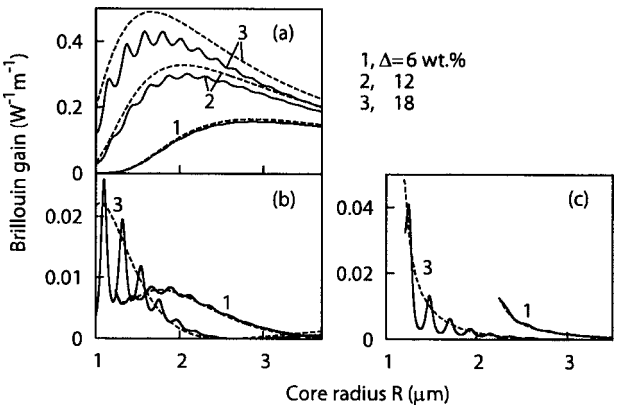

Fig. 2. (a)–(c) Brillouin gain coefficient g_η for modes LR_1-LR_3 as a function of core radius for different doping concentrations Δ at acoustic frequency 10 GHz. Solid and dashed curves show the cases $V_{S1} \neq V_{S2}$ and $V_{S1}=V_{S2}$, respectively.

For the steady state ($\partial_t a_j \approx 0$) and undepleted ($\partial_z a_p \approx 0$) regime, the gain spectral profile has the form $g_B(\omega_q)=\Sigma_\eta g_\eta(\Gamma_\eta'/2)^2/[(\Gamma_\eta'/2)^2+(\Omega_{B\eta}-\omega_q)^2]$, which is a sum of different Lorentzian functions of centers $\Omega_{B\eta}$ and linewidth $\Gamma_\eta'/2$, with the gain coefficient $g_\eta=(\gamma^2 k_p^3\beta_\eta^2/8c\beta_p^2\rho_0\omega_q\Gamma_\eta')|\int_0^\infty F^2F_\eta r\,dr|^2$. From Eqs. (1) and (2), we obtain

$$[\partial_z + (\bar{n}/c)\partial_t]a_s = a_p \sum_\eta g_\eta w_\eta^*(z,t),$$

$$[\partial_z - (\bar{n}/c)\partial_t]a_p = a_s \sum_\eta g_\eta w_\eta(z,t), \quad (3)$$

where $w_\eta(z,t)=(\Gamma_\eta'/2)\int_0^t \exp[\Gamma_\eta(t-\tau)]a_p a_s^*\,d\tau$ and $\bar{n}$ is the averaged refractive index. Equations (3) are obtained similarly for the Brillouin interaction of different optical modes in free space.[11]

Figure 2 shows the SBS gain coefficient g_{1-3} for the interaction of the optical mode with acoustic modes LR_1-LR_3 as a function of the core radius for different GeO_2 concentrations. In comparison, the gain is lower for $V_{S1} \neq V_{S2}$ than for $V_{S1}=V_{S2}$, except for LR_2 and LR_3 modes at some small core radii [Figs. 2(b) and 2(c)]. The shift in the maximum of g_1 to larger core radii for smaller dopings [Fig. 2(a)] is due to the spreading of the optical mode in the transverse directions. For the steady-state and undepleted regime of SBS the exponential growth of the Stokes power is $\exp(g_\eta|a_p|^2L)$, where $|a_p|^2$ is the pump power and L is the interaction length. Using g_{1-3} in Fig. 2, the threshold power for different modes can be estimated as $|a_p|_{th}^2 \simeq 21/g_\eta L$, and hence the parameter set for the lowest or highest threshold powers of LR_1-LR_3 modes can be identified.

The Brillouin frequencies of LR_1–LR_3 modes are shown as a function of the core radius for various GeO_2 concentrations in Fig. 3(a). The separation of Ω_{B1}, Ω_{B2}, and Ω_{B3} is reduced for larger core radii, resulting in merging of higher-order peaks into the main Brillouin peak. Smaller core radii, however, result in a bigger separation of the Brillouin frequencies, which is advantages for those applications that require distinct Brillouin peaks. An important practical aspect of Fig. 3(a), which can be used for simultaneous strain and temperature sensing, is that for a large core radius, 3.0 μm, the slopes of the Brillouin frequency versus doping are almost the same for LR_1 and LR_2, 72.0, and 71.5 MHz/wt. % respectively, whereas for a small core radius, 1 μm, they are different, 76.0 and 69.0 MHz/wt. %, respectively [Fig. 3(b)]. As a result, LR_1 and LR_2 modes of small-core-radius fibers (close to the cutoff of LR_2 mode) have different sensitivities to variation of the refractive index and the speed of sound, which change linearly with doping. Thus, the parameter regime close to the cutoff region of LR_2 or LR_3 modes is preferable for simultaneous strain and temperature measurements.

We note that the parameter set $R=1.5$ μm and doping $\Delta=6$ wt. %, which are in the vicinity of the cutoff region of the LR_2 mode, result in the maximum relative gain of LR_2/LR_1 mode ≈ 0.21. However, this ratio is valid for the undepleted regime and can be improved significantly by choosing values of pump and probe powers and interaction length resulting in pump depletion. Although the developed transient model is applicable to sub-10-ns pulses, to demonstrate the depletion effect and have distinctive peaks in BGS we choose a 30 ns pulse with a large cw base,[12] since shorter pulses result in broadened and merged peaks. Comparing curves 1 and 3 in Fig. 4, obtained by solving Eqs. (3) for the same pump and probe powers but different interaction lengths of 1 and 800 m, it is evident that there is an improvement of the ratio of LR_2 to LR_1 peaks from 0.27 to 0.67 for the longer interaction length. For curve 4, we kept the interaction length as 800 m but reduced the pulse and its base powers. Comparing the peak ratio of LR_2 over LR_1 for curves 4 and 3, which are 0.21 and 0.67, respectively, indicates a higher ratio for a higher probe power. This is expected, since the exponential growth of the Stokes power is valid for the undepleted regime only, whereas for large values of the pump powers or long fibers the pump depletes considerably, resulting in saturation. Because values of g_{1-3} are different, there is a parameter set close to the saturation growth regime of LR_1 mode, but the exponential growth regime of higher-order modes results in the enhancement of the peak ratio of the LR_2 over the LR_1 mode.

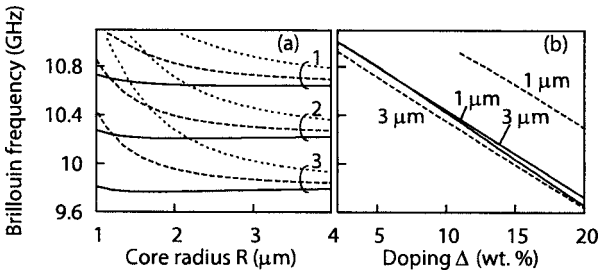

Fig. 3. Brillouin frequencies of (solid) LR_1, (dashed) LR_2, and (dotted) LR_3 modes as a function of (a) core radius and (b) doping. The labels 1, 2 and 3 in (a) refer to the same dopings as Fig. 2, and the core radii in (b) are as indicated.

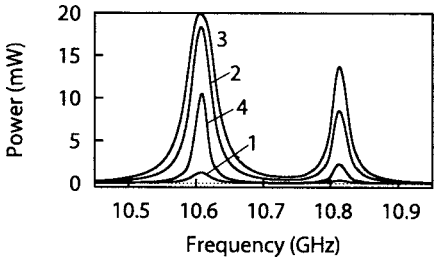

Fig. 4. (a) Pump power loss versus frequency of a fiber with $R=1.5$ μm and $\Delta=6$ wt. % for a 20 mW pump. The probe beam contains a 100 mW (peak power) pulse and 50 mW cw base (curves 1–3) and a 10 mW pulse and 5 mW cw base (curve 4). The interaction lengths are (1) 1 m, (2) 400, and (3–4) 800 inside an 800 m fiber.

We thank the National Capital Institute of Telecommunications, Intelligent Sensing for Innovative Structures, Natural Science and Engineering Research Council, and Research Chair Program, Canada for their support. S. Afshar's and V. Kalosha's email addresses are shahraam.afshar@adelaide.edu.au and vladimir.kalosha@science.uottawa.ca.

*Present address, Centre of Expertise in Photonics, University of Adelaide, Adelaide, SA5005, Australia.

References

1. X. Bao, D. J. Webb, and D. A. Jackson, Opt. Lett. **18**, 552 (1993).
2. M. Nikles, L. Thevenaz, and P. A. Robert, J. Lightwave Technol. **15**, 1841 (1997).
3. A. Yeniay, J.-M. Delavaux, and J. Toulouse, J. Lightwave Technol. **20**, 1425 (2002).
4. C. C. Lee, P. W. Chiang, and S. Chi, IEEE Photon. Technol. Lett. **13**, 1094 (2001).
5. L. Zou, X. Bao, S. Afshar V., and L. Chen, Opt. Lett. **29**, 1485 (2004).
6. N. Shibata, K. Okamoto, and Y. Azuma, J. Opt. Soc. Am. B **6**, 1167 (1989).
7. J. W. Yu, Y. Park, K. Oh, and I. B. Kwon, Opt. Express **10**, 996 (2002).
8. Y. Koyamada, S. Sato, S. Nakamura, H. Sotobayashi, and W. Chujo, J. Lightwave Technol. **22**, 631 (2004).
9. N. Lagakos, J. A. Bucaro, and R. Hughes, Appl. Opt. **19**, 3668 (1980).
10. R. A. Waldron, IEEE Trans. Microwave Theory Tech. **17**, 893 (1969).
11. S. Afshaarvahid and J. Munch, J. Nonlinear Opt. Phys. Mater. **10**, 1 (2001).
12. S. Afshar V., G. A. Ferrier, X. Bao, and L. Chen, Opt. Lett. **28**, 1418 (2003).